Entropy driven stability of chiral single-walled carbon nanotubes

Yann Magnin, Hakim Amara, François Ducastelle, Annick Loiseau, Christophe Bichara

Entropy driven stability of chiral single-walled carbon nanotubes

Y. Magnin,[1] H. Amara,[2] F. Ducastelle,[2] A. Loiseau,[2] and C. Bichara*[1]

[1]*Centre Interdisciplinaire de Nanoscience de Marseille, Aix-Marseille University and CNRS, Campus de Luminy, Case 913, F-13288, Marseille, France.*

[2]*Laboratoire d'Etude des Microstructures, ONERA-CNRS, BP 72, F-92322, Châtillon, France.*

Abstract

Single-walled carbon nanotubes are hollow cylinders, that can grow centimers long by carbon incorporation at their interface with a catalyst. They display semi-conducting or metallic characteristics, depending on their helicity, that is determined during their growth. To support the quest for a selective synthesis, highly desirable for applications, we develop a thermodynamic model, that relates the tube-catalyst interfacial energies, temperature, and the resulting tube chirality. We show that nanotubes can grow chiral because of the configurational entropy of their nanometer-sized edge, thus explaining experimentally observed temperature evolutions of chiral distributions. Taking the chemical nature of the catalyst into account through interfacial energies, structural maps and phase diagrams are derived, that will guide a rational choice of a catalyst and growth parameters towards a better selectivity.

Synthesizing carbon nanotubes pushes crystal growth to its size limit. Like nanowires[1], carbon nanotubes are fed during growth from their interface with a catalyst[2]. Nanowire interfaces are large, in the 10-50 nm diameter range, while single-walled nanotubes (SWNT) have smaller diameter, and, in some cases, the contact between the tube and its seeding particle is reduced to a line, with typically 10-50 carbon atoms. Such a linear interface is simple to deal with, and we propose here a thermodynamic model of the interface, from which we derive structural maps and phase diagrams linking catalyst properties, experimental conditions, and the corresponding stable tube structure, characterized by its (n, m) chiral indexes. This will provide a rational basis for the quest of a selective growth of SWNTs. Indeed, a growing number of potential applications require control over the metallic or semi-conducting properties of SWNTs. Among these, the use of SWNT yarns as strong, light and conductive wires is a promising perspective[3], but the next major challenge is to develop SWNT-based electronics [4], with the ultimate goal of overcoming the limitations of silicon. Significant breakthroughs have been reported [5] and progress towards Carbon Nanotube computers [6, 7] has been very rapid. In this chain of substantial steps forward, selective synthesis still appears to be the weak link, though new experiments using solid state catalysts[8–10] have reported a chiral specific growth of SWNTs. Detailed mechanisms underlying this selective growth are still debated, and the resulting (n, m) tube structures difficult to interpret, thus underlining the need for a realistic model including the role of the catalyst. Existing growth models either focus on kinetics [11], or neglect the role of the catalyst [12], or combine thermodynamics and kinetics [13], but fail to calculate chiral distributions in line with experiments. Atomistic computer simulations are often preferred [14, 15], giving invaluable atomic scale insights, but need to be complemented with a model so as to provide a global understanding of the process.

In order to build such a model, we start by recalling some experimental evidences. Vapor Liquid Solid and Vapor Solid Solid Chemical Vapor Deposition (CVD) processes have been identified [9], the latter leading to a (n, m) selectivity. Growth can proceed through tangential or perpendicular modes[16], and ways to control them have been proposed quite recently[17]. For specific catalysts and growth conditions favoring the perpendicular mode, a pronounced near armchair selectivity can be observed [17]. In such a mode, the interface between the tube and the catalyst nanoparticle (NP) is limited to a line, and a simple model describing the thermodynamic stability of the tube-nanoparticle system can be developed. We thus consider an ensemble of configurations of a catalyst NP, possibly a metal or a carbide, in perpendicular contact with a (n, m) SWNT, as

in Figure 1. The total numbers of carbon and catalyst atoms are constant. Configurations differ by the structure of the NP-tube interface, defined by (n, m), for which we have $(n + m)$ SWNT-NP bonds, with typically $10 < n + m < 50$. On the tube edge, $2\,m$ among them are armchair, and $(n - m)$ zigzag [18]. In a first approximation, the atomic structure of the NP is neglected, and the catalyst appears as a smooth flat surface, in a jellium-like approximation. The interface is then a simple closed loop with two kinds of species: armchair and zigzag contact atoms. Under these conditions, the total energy of the system can be split in three terms:

$$E(n, m) = E_0 + E_{curv}(n, m) + E_{Int}(n, m), \tag{1}$$

where E_0 includes all terms independent of (n, m), such as the energy of the 3-fold coordinated carbon atoms in the tube wall, and the atoms forming the NP. The surface energy of the NP and the very weak surface energy of the tube are also included in E_0, because these surfaces are kept constant. Note that this model could possibly apply also in tangential mode, if the lateral tube/catalyst interaction does not depend on (n, m).

The (n, m) dependent energy terms concern the tube curvature, and its interface with the NP. Using Density Functional Theory (DFT) calculations, Gülseren *et al.* [19] evaluated the curvature energy of the isolated tube as $E_{curv} = 4\alpha D_{CNT}^{-2}$, D_{CNT} being the tube diameter, and $\alpha = 2.14 eV\mathring{A}^2$ / C atom. We assume that the interfacial energy for a (n, m) tube in contact with the NP surface depends only on the number of its $2\,m$ armchair and $(n - m)$ zigzag contacts:

$$E_{Int}^{(n,m)} = 2\,m\,E_{Int}^{A} + (n - m)\,E_{Int}^{Z} \tag{2}$$

where the armchair (E_{Int}^{A}) and zigzag (E_{Int}^{Z}) interfacial energies are given by $E_{Int}^{X} = \gamma_G^X + E_{Adh}^X$, with X standing for A or Z. The edge energy per dangling bond, γ_G^X, is positive since it is the energy cost of cutting a tube or a graphene ribbon, and depends on the type of edge created. The adhesion energy of the tube in contact with the NP, E_{Adh}, is negative since energy is gained by reconnecting a cut tube to the NP. E_{Int}, sum of these two terms has to be positive to create a driving force for SWNT formation. In a simple approximation, supported by DFT calculations reported in Figure 2-b, no ordering effects are taken into account in equation 2, meaning that all tube catalyst interfaces with the same number of armchair and zigzag contacts have the same energy.

This leads us to introduce the edge configurational entropy as a central piece of the model. We assume that the tube is cut almost perpendicular to its axis, forming the shortest possible interface, for a given (n, m). We neglect vibrational entropy contributions, that are essentially the same for

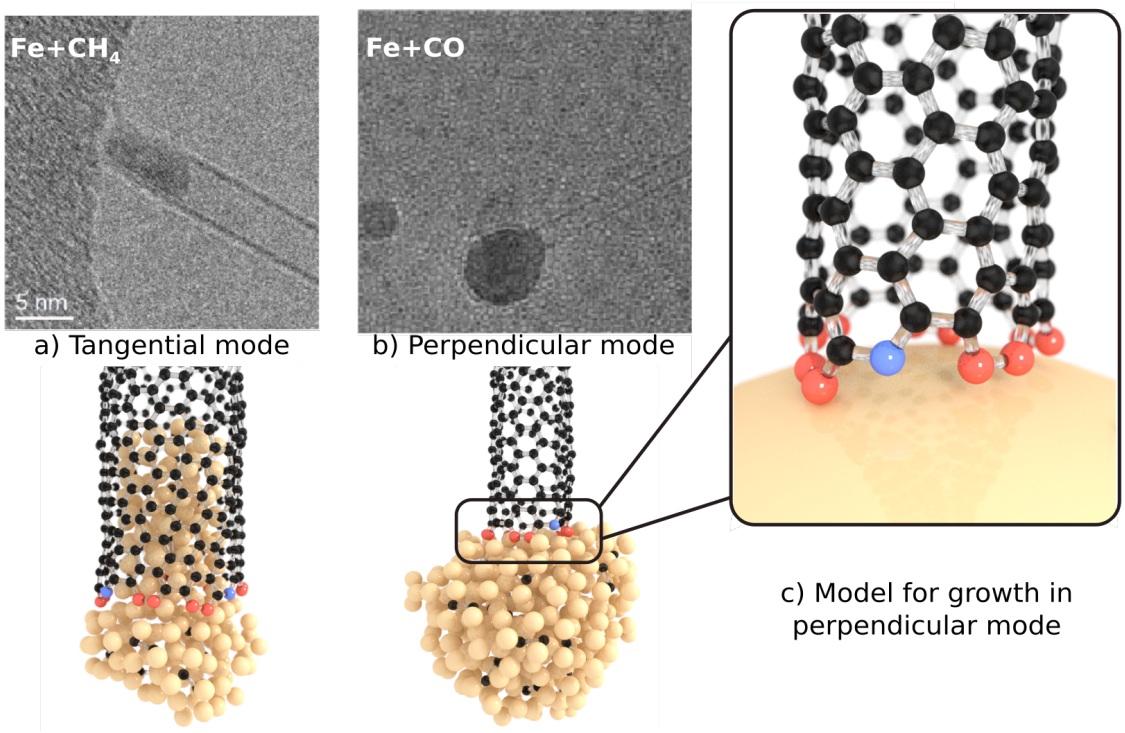

FIG. 1. (Color online) **From experiments to a model**. Top: post-synthesis TEM images of a SWNT attached to the nanoparticle from which it grew at 1073 K, using either CH_4 **(a)**, or CO **(b)** carbon feedstocks, leading to tangential or perpendicular growth mode ([17]), illustrated at the atomic scale in the bottom line. Sketch of the model **(c)**, with a SWNT in perpendicular contact with a structureless catalyst. Armchair edge atoms are in red, zigzag ones in blue.

all tubes, except for radial breathing modes. Noting that armchair 2-fold coordinated C atoms always come by pair, this entropy, related to the number of ways of putting $(n-m)$ zigzag C atoms and m pairs of armchair atoms on n sites (degeneracy) writes:

$$\frac{S(n,m)}{k_B} = \ln\left(\frac{n!}{m!(n-m)!}\right) \approx -n\left(c\ln c + (1-c)\ln(1-c)\right) \tag{3}$$

where $c = m/n$, the fraction of armchair pairs, is reminiscent of the mole fraction in a regular solution model.

Interfacial energies can be evaluated using DFT calculations, described in Supplementary Materials. In agreement with[18, 20], we find $\gamma_G^A = 2.06$ eV / bond and $\gamma_G^Z = 3.17$ eV / bond for graphene, and 1.99 and 3.12 respectively for cutting $(6,6)$ and $(12,0)$ tubes. The lower value of γ_G^A is due to the relaxation (shortening) of the C-C bonds of the armchair edge that stabilizes it. Adhesion energies of (10,0) and (5,5) tubes on icosahedral clusters of various metals, including

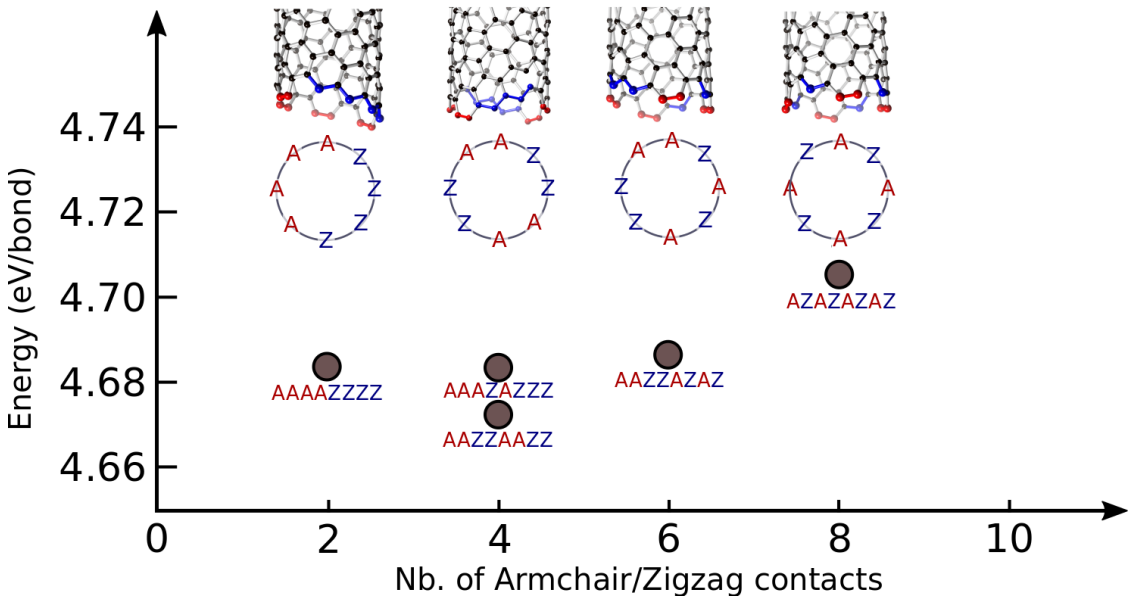

FIG. 2. (Color online) **Key elements of the model**. **Top** Different ways of cutting a $(8,4)$ tube, leading to the formation of zigzag (blue) and armchair (red) undercoordinated atoms. For a $(8,4)$ tube, there are 70 different edge configurations with almost the same energy. **Bottom** Formation energies of all possible $(8,4)$ edges, from DFT calculations described in Methods. They lie within 25 meV / bond, and can thus be considered degenerate.

Fe, Co, Ni, Cu, Pd and Au were calculated in [21, 22]. Thus, orders of magnitude for interface energies, E_{Int}, of armchair and zigzag terminations in contact with these metals can be estimated: they typically lie between 0.0 and 0.5 eV / bond, with $E^A_{Int} < E^Z_{Int}$ for these metals. Examples of free energies, and corresponding probability distributions are plotted as a function of (n,m) in Figures S1.

Instead of focusing on a specific catalytic system, it is more relevant at this stage to study the general properties of the model that links the (n,m) indexes of a SWNT, to three parameters characterizing its CVD growth conditions, namely temperature and the interfacial energies of armchair (E^A_{Int}) and zigzag (E^Z_{Int}) tube-catalyst contacts. For each set of parameters, a free energy can be calculated, and its minimization yields the stable (n,m) value. This model displays similarities with a simple alloy model on a linear chair, but the curvature term, dominant for small diameters, and the small and discrete values of n and m, prevent to make it analytically solvable, except for ground states, i.e. stable structures at zero Kelvin, for which a solution is provided in Methods.

We thus define a 3-dimensional space of stable configurations in the (T, E^A_{Int}, E^Z_{Int}) coordinates.

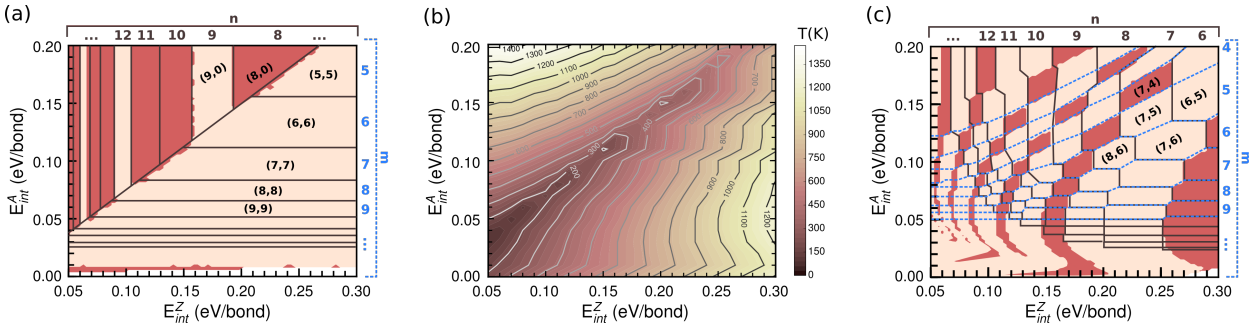

FIG. 3. (Color online) **Structural maps**. **a)** Map of the ground states, with armchair tubes in the lower right corner, and zigzag ones in the upper left corner, separated by a line $E^Z_{Int} = 4/3E^A_{Int}$. Small diameter tubes, e.g. $(5,5)$ and $(8,0)$, are obtained for large values of the interfacial energies E_{Int}, while stability domains of large diameter tubes are narrower, with a width decaying as $\frac{1}{n(n+1)}$, and obtained for small values of E_{Int}. **b)** Contour plot of the highest temperatures of stability of the ground state structures, armchair or zigzag. Chiral tubes are only found above this surface, stabilized by the configurational entropy of the tube's edge. Note that armchair and zigzag tubes can remain stable at high temperatures, in the bottom right and upper left corners respectively. **c)** Chirality map at 1000 K. Iso-n (resp. iso-m) values are delimited by full black (resp. dashed blue) lines. Metallic tubes, for which $(n-m)$ is a multiple of 3, are shown in brick red, and semi-conducting ones are flesh-colored. The parameter space for armchair (metallic) and $(n, n-1)$ and $(n, n-2)$ (semi-conducting) tubes is larger than for other chiralities.

Setting T, and hence the entropy contribution to zero, the ground states are readily calculated and displayed in Figure 3-a. Interestingly, only armchair or zigzag tubes are found to be stable, separated by a line $E^Z_{Int} = 4/3E^A_{Int}$. With increasing temperature, they become unstable, and a transition towards chiral tubes takes place. Figure 3-b is a contour plot of the surface defined by the transition temperatures. Above this surface, for each set of $(E^A_{Int}, E^Z_{Int}, T)$ parameters, a chiral (n, m) tube is found stable, defining "volumes" of stability for each chirality. To explore it, we can either cut slices at constant temperature to obtain an isothermal stability map (Figure 3-c), or fix either E^A_{Int} or E^Z_{Int} to obtain temperature dependent "phase diagrams", as in Figures 4-a (for E^A_{Int} = 0.15 eV / bond) and 4-b (for E^Z_{Int} = 0.25 eV / bond). As an example, we can follow the temperature stability of a $(6,6)$ tube. Figure 4-a shows a large stability range with a maximal stability temperature rising from 200 to 800 K by increasing E^Z_{Int} from 0.20 to 0.30 eV / bond,

whereas the second map, orthogonal to the first one in the 3-d configuration space, shows an upper temperature limit varying from 500 to 700 K, within a narrower E_{Int}^{A} range. Above the armchair tubes, chiral $(n, n-m)$ tubes become stable starting with $(n, n-1)$, and then with increasing $n-m$ values such as (6,5), (7,5), etc ... A first and important result is that chiral tubes, i.e. tubes different from armchair or zigzag, are stabilized at finite temperature by the configurational entropy of the tube edge.

An isothermal map calculated at 1000 K is plotted in Figure 3-c. Chiral tubes are spread along the $E_{Int}^{Z} = 4/3E_{Int}^{A}$ diagonal, between armchair and zigzag ones. Small diameter tubes are stabilized for larger values of $(E_{Int}^{A}, E_{Int}^{Z})$, hence for weaker adhesion energies of the tube on the catalyst. Larger diameter tubes are obtained for small values of $(E_{Int}^{A}, E_{Int}^{Z})$, because the entropy cannot counterbalance the energy cost of the interface, proportional to $(n + m)$, if interfacial energies are too large. A comparison of maps at 1000 to 1400 K is given in Figure S2. The effect of increasing temperature is to expand and shift the stability domain of chiral tubes, with a trend to favor central $(2n, n)$ chiralities. We note however that the free energy differences become smaller, thus explaining the lack of selectivity reported for tubes grown at very high temperature by electric arc or laser ablation methods [23].

This very simple model has the advantage of a great physical transparency and displays a fair agreement with literature data, as illustrated in the following examples. Figure 3-b, suggests a way to grow either zigzag or armchair tubes, the latter being metallic for any diameter. For both, growth kinetics is slow, because each new ring of carbon atoms has to nucleate, once the previous one has been completed [12, 13]. To overcome this nucleation barrier, one should seek regions in the map, where such tubes remain stable at high temperature. For armchair species, this corresponds to the lower right corner of the map in Figure 3-b, where the adhesion energy of armchair edges is strong, and that of zigzag ones is weak, and the contrary for the interfacial energies. Such requirements have possibly been met in the high temperature (1473 K) CVD experiments reported in [24], that also used thiophene in the feedstock. Those experiments, still unreproduced, might indicate that the presence of sulfur at the interface could modify the relative interaction strength of zigzag and armchair edges with the Fe NP. The temperature dependence of the chiral distribution, measured by photoluminescence in [25], [26] and [27], and Raman and Transmission Electron spectrocopies in [28] seems more robust. The maps presented in Figures 4-a and 4-b are quite consistent with these experiments showing that armchair or near armchair chiralities -$(6, 6)$ and $(6, 5)$- are grown at low temperature (873 K), and that the chiral distribution gradually shifts towards larger chiral

angles -$(7,5)$, $(7,6)$ and $(8,4)$, ...- at higher temperatures. Referring to our model, this suggests that Co and Fe based catalysts used in these experiments correspond to interfacial energy values around $E^A_{Int} = 0.15$ and $E^Z_{Int} = 0.20$ eV / bond, as indicated by the dashed boxes in the maps. Our results also indicate that a large fraction of metallic tubes with neigboring helicities -$(6,6)$ and $(7,4)$-, not detectable by photoluminescence, should also be present in references [25] and [27].

The present model thus sets a global framework for understanding why a number of experiments, using metallic catalysts in perpendicular growth conditions, as discussed in [17], report a near armchair selectivity. For such catalysts, E^A_{Int} is generally lower than E^Z_{Int}[21]. At low temperature, zigzag or armchair tubes are thermodynamically favored, but may not always be obtained due to kinetic reasons. On the armchair side, our model indicates that close to armchair helicities are then favored by a temperature increase, because their stability domain is large, and they are less kinetically impaired[12]. At even higher temperatures, tube chiralities tending towards $(2n,n)$ indexes, should be stabilized by their larger edge configurational entropy, but their stability domains turn out to be narrower in the present model. Taking the atomic structure of the catalyst into account in our model could rule out some neighboring structures, and contribute to open up these domains.

Concerning the practical use of these maps, a first issue is to select the appropriate location for a catalyst in the $(E^A_{Int}, E^Z_{Int}, T)$ coordinates, so as to obtain the desired tube helicity. Growing, on demand, SWNTs with metallic or semi-conducting tubes is the central point. Looking at Figure 3-c, one can see that the largest and most interesting parameter ranges correspond to either metallic armchair tubes, or to $(n, n-1)$ and $(n, n-2)$ semi-conducting tubes. The second, more difficult issue is to design a catalyst that would display appropriate E^A_{Int} and E^Z_{Int} values. DFT-based calculations, in the same spirit as those in [8, 10, 21, 22, 29] should probably be helpful. Note however that the argument of lattice or symmetry matching between the tube and the catalyst [8, 10] is somewhat irrelevant, since it is clear that a chiral tube cannot preserve the symmetry of its interface during growth, for the same reason that leads to the significant edge configurational entropy. This intrinsic disorder should be taken into account by averaging over various atomic configurations, and using Molecular Dynamics at finite temperature. By providing a rational basis for the choice of an appropriate catalyst, the present work paves the way towards an efficient selective SWNT growth. The key is now to find a practical way to tune the relative interaction of zigzag and armchair edges with respect to the catalyst. In view of the huge investments already made on SWNT growth, and of the potential rewards of selective growth, a smart combination of

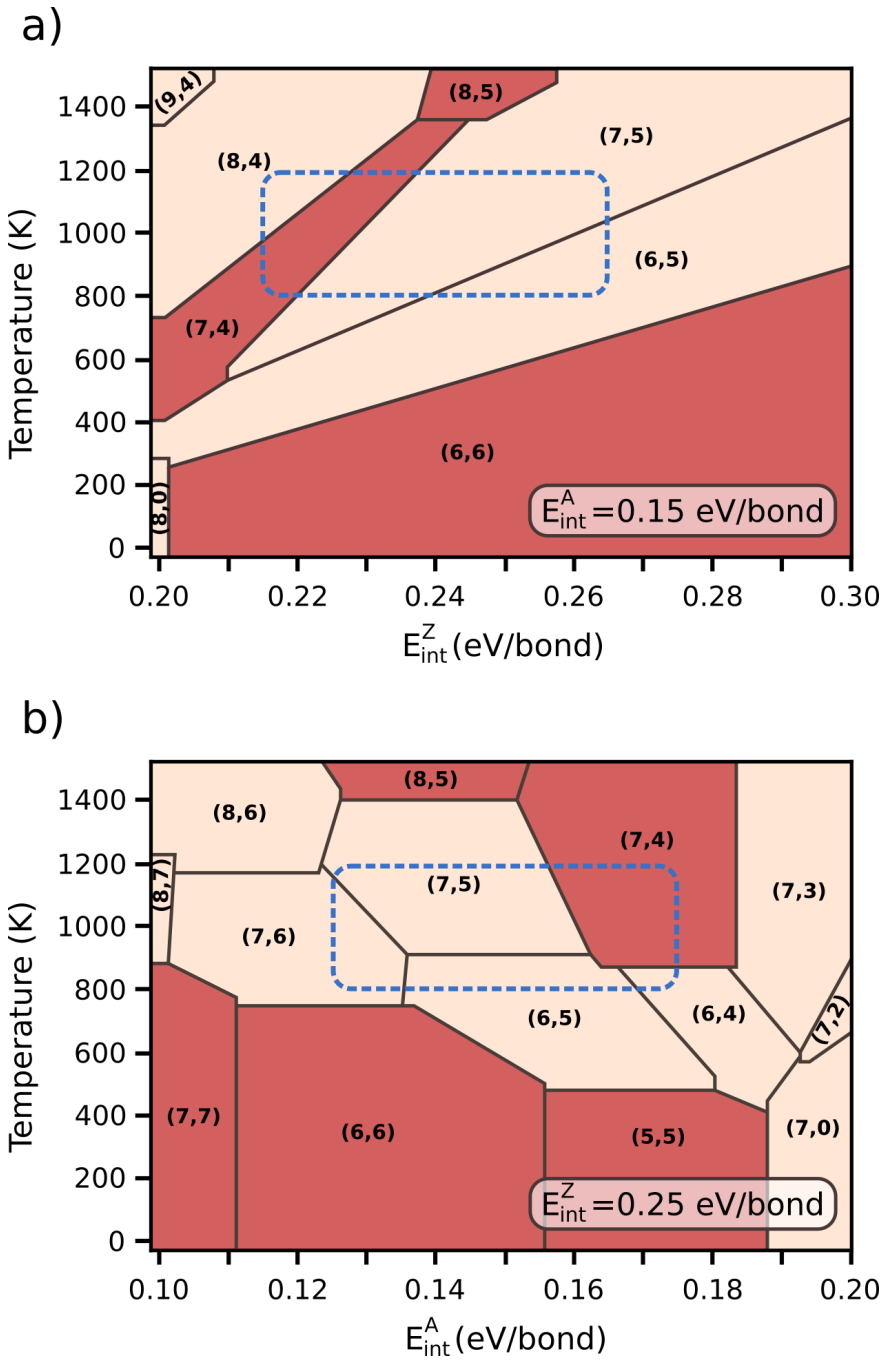

FIG. 4. (Color online) **Chirality phase diagrams**. Phase diagrams calculated for constant values of E^A_{Int} (**a**) and E^Z_{Int} (**b**). These diagrams would be orthogonal in a 3-dimensional plot. The blue dashed boxes indicate possible parameter ranges corresponding to the analysis of growth products by He *et al.*[27], based on a photoluminescence assignment of tubes grown using a FeCu catalyst. $(6,5)$ are reported stable up to 1023 K, $(7,5)$ and $(8,4)$ become dominant at 1023 K, and $(7,6)$ at 1073 K.

chemical intuition, supported by computational screening, and careful, innovative catalyst choice should make it possible.

More fundamentally, the present model opens a new understanding of SWNT growth mechanisms. The intrinsic interfacial disorder, reflected by the importance of the entropy of the tube edge, raises questions regarding the possibility to control the growing tube structure through a crystalline structure of the catalyst. More than the crystallinity of the catalyst interface with the tube, unlikely under growth conditions, our approach emphasizes the role of the chemical bonding at the interface. This bonding between armchair or zigzag tube edges and the surface atoms of the catalyst depends primarily on their local order, that is the type and organization of chemical bonds formed. Another aspect is that the present model, purely based on a thermodynamic approach, accounts for experimental evidences, such as a close to armchair preferential selectivity, hitherto attributed to kinetics[12], the importance of choosing an appropriate catalyst, and the temperature dependent trends in chiralities. While kinetics can drive the structure of nanowires[1], there might be SWNT growth regimes where the atomic mobility and the residence time of atoms close to the interface are large enough to achieve a local thermodynamic equilibrium, favored by the extremely small size of the interface, and the high temperature. This makes SWNT synthesis a very special case in crystal growth and catalysis.

---

[1] S. Hofmann, R. Sharma, C. T. Wirth, F. Cervantes-Sodi, C. Ducati, T. Kasama, R. E. Dunin-Borkowski, J. Drucker, P. Bennett, and J. Robertson, Nat. Mater. **7**, 372 (2008).

[2] V. Jourdain and C. Bichara, Carbon **58**, 2 (2013).

[3] N. Behabtu, C. C. Young, D. E. Tsentalovich, O. Kleinerman, X. Wang, A. W. K. Ma, E. A. Bengio, R. F. ter Waarbeek, J. J. de Jong, R. E. Hoogerwerf, S. B. Fairchild, J. B. Ferguson, B. Maruyama, J. Kono, Y. Talmon, Y. Cohen, M. J. Otto, and M. Pasquali, Science **339**, 182 (2013).

[4] A. D. Franklin, Nature **498**, 443 (2013).

[5] Q. Cao, S.-J. Han, J. Tersoff, A. D. Franklin, Y. Zhu, Z. Zhang, G. S. Tulevski, J. Tang, and W. E. Haensch, Science **350**, 68 (2015).

[6] M. M. Shulaker, G. Hills, N. Patil, H. Wei, H.-Y. Chen, H.-S. P. Wong, and S. Mitra, Nature **501**, 526 (2013).

[7] M. M. Shulaker, G. Hills, R. S. Park, R. T. Howe, K. Saraswat, H.-S. P. Wong, and S. Mitra, Nature

547, 74 (2017).

[8] F. Yang, X. Wang, D. Zhang, J. Yang, D. Luo, Z. Xu, J. Wei, J.-Q. Wang, Z. Xu, F. Peng, X. Li, R. Li, Y. Li, M. Li, X. Bai, F. Ding, and Y. Li, Nature **510**, 522 (2014).

[9] M. Li, X. Liu, X. Zhao, F. Yang, X. Wang, and Y. Li, Top. Curr. Chem. **375**, 29 (2017).

[10] S. Zhang, L. Kang, X. Wang, L. Tong, L. Yang, Z. Wang, K. Qi, S. Deng, Q. Li, X. Bai, F. Ding, and J. Zhang, Nature **543**, 234 (2017).

[11] A. A. Puretzky, D. B. Geohegan, S. Jesse, I. Ivanov, and G. Eres, Appl. Phys. A **81**, 223 (2005).

[12] F. Ding, A. R. Harutyunyan, and B. I. Yakobson, Proc. Natl. Acad. Sci. **106**, 2506 (2009).

[13] V. I. Artyukhov, E. S. Penev, and B. I. Yakobson, Nat. Commun. **5**, 4892 (2014).

[14] A. J. Page, F. Ding, S. Irle, and K. Morokuma, Rep. Prog. Phys. **78**, 036501 (2015).

[15] H. Amara and C. Bichara, Top. Curr. Chem. **375**, 55 (2017).

[16] M. F. C. Fiawoo, A. M. Bonnot, H. Amara, C. Bichara, J. Thibault-Pénisson, and A. Loiseau, Phys. Rev. Lett. **108**, 195503 (2012).

[17] M. He, Y. Magnin, H. Jiang, H. Amara, E. I. Kauppinen, A. Loiseau, and C. Bichara, submitted to Nanoscale, available on arXiv:1802.04029 (2018).

[18] Y. Liu, A. Dobrinsky, and B. I. Yakobson, Phys. Rev. Lett. **105**, 235502 (2010).

[19] O. Gülseren, T. Yildirim, and S. Ciraci, Phys. Rev. B **65**, 153405 (2002).

[20] T. Wassmann, A. Seitsonen, A. M. Saitta, M. Lazzeri, and F. Mauri, Phys. Rev. Lett. **101**, 096402 (2008).

[21] F. Ding, P. Larsson, J. Andreas Larsson, R. Ahuja, H. Duan, A. Rosen, and K. Bolton, Nano Lett. **8**, 463 (2008).

[22] A. Börjesson and K. Bolton, J. Phys. Chem. C **114**, 18045 (2010).

[23] L. Henrard, A. Loiseau, C. Journet, and P. Bernier, Eur. Phys. J. B **13**, 661 (2000).

[24] R. M. Sundaram, K. K. K. Koziol, and A. H. Windle, Adv. Mater. **23**, 5064 (2011).

[25] X. L. Li, X. Tu, S. Zaric, K. Welsher, W. S. Seo, W. Zhao, and H. Dai, J. Am. Chem. Soc. **129**, 15770 (2007).

[26] H. Wang, B. Wang, X.-Y. Quek, L. Wei, J. Zhao, L.-J. Li, M. B. Chan-Park, Y. Yang, and Y. Chen, Journal of the American Chemical Society **132**, 16747 (2010).

[27] M. He, A. I. Chernov, P. V. Fedotov, E. D. Obraztsova, J. Sainio, E. Rikkinen, H. Jiang, Z. Zhu, Y. Tian, E. I. Kauppinen, M. Niemela, and a. O. I. Krause, J. Am. Chem. Soc. **132**, 13994 (2010).

[28] M. Fouquet, B. C. Bayer, S. Esconjauregui, R. Blume, J. H. Warner, S. Hofmann, R. Schlögl, C. Thom-

sen, and J. Robertson, Phys. Rev. B **85**, 235411 (2012).

[29] F. Silvearv, P. Larsson, S. L. T. Jones, R. Ahuja, and J. A. Larsson, J. Mater. Chem. C **3**, 3422 (2015)

.

SUPPLEMENTARY MATERIAL OF : ENTROPY DRIVEN STABILITY OF CHIRAL SINGLE-WALLED CARBON NANOTUBES.

DFT calculations

The first-principles code Quantum Espresso [1] employing density functional theory (DFT) within the projector-augmented wave (PAW) method [2] is used to calculate the formation energies of all possible (8, 4) edges. The generalized gradient approximation (GGA) [3] is employed for the exchange and correlation energy terms. We use a periodic cell allowing for 20 Å vacuum between the nanotubes to avoid interaction between neighboring supercells. Integrations over the Brillouin zone are based on a (1x1x5) Monkhorst-Pack three-dimensional grid for cells containing a tube of 150 to 200 atoms along the c axis. Cold smearing is used for the Brillouin zone integration leading to formation energies converged to within 10^{-6} eV. The cell is kept fixed and the atomic positions are relaxed using the conjugate gradient minimization scheme until the magnitude of the forces on all the atoms are smaller than 0.04 Ry/au.

Thermodynamic model

The free energy $\hat{F}(n, m, T)$ of the system includes three (n, m) dependent terms :

$$\begin{aligned} E_{Int} &= (n-m)E^{Z}_{Int} + 2mE^{A}_{Int} \\ E_{curv} &= 4\alpha D^{-2}_{CNT} \\ -k_B T S &= -k_B T \ln\left(\frac{n!}{m!(n-m)!}\right) \\ &\simeq k_B T\left[m\log m + (n-m)\log(n-m) - n\log n\right] \end{aligned}$$

The tube diameter is related to its (n, m) index by the relation $D_{CNT} = \sqrt{3}d_{CC}\sqrt{n^2+nm+m^2}$ where $d_{CC} = 1.42$ Å is the C-C bond distance. E_{curv} can be written $K(n+m)/(n^2+nm+m^2)$ where $K = (4\alpha)/(3d^2_{CC})$. Therefore, $\hat{F}(n, m, T)$ writes :

$$\hat{F}(n, m, T) = (n-m)E^{Z}_{Int} + 2mE^{A}_{Int} + K(n+m)/(n^2+nm+m^2) \quad (4)$$

$$+ k_B T \left[m \log m + (n-m) \log(n-m) - n \log n \right] .$$

For each set of $(E^A_{Int}, E^Z_{Int}, T)$ the (n, m) set corresponding to the most stable SWNT is obtained by minimizing the free energy $\hat{F}(n, m, T)$ with respect to n and m. This minimization can be performed numerically in a straightforward way, leading to the results at non-zero temperature presented in the body of the paper. For the sake of completeness, and for a better physical insight, an analytical solution can be developed, though approximately at non-zero temperature.

Analytical solution for ground states

To minimize the energy at zero Kelvin, it is convenient, in a first step, to consider n and $c = m/n$ as continuous variables, with $0 \leq c \leq 1$. Equation 4 becomes :

$$\hat{F}(n, c, T = 0) = n\tilde{E}(c) + \frac{1}{n} \tilde{K}(c) , \tag{5}$$

with:

$$\tilde{E}(c) = 2cE^A_{Int} + (1-c)E^Z_{Int} \quad (E^A_{Int}, E^Z_{Int} > 0)$$
$$\tilde{K}(c) = K \frac{1+c}{1+c+c^2} \quad (K > 0)$$

We omit $T = 0$ and now have to minimize $\hat{F}(n, c)$ with respect to n and c. From $\partial \hat{F}/\partial n = 0$, we obtain $n^2 = \tilde{K}(c)/\tilde{E}(c)$, hence :

$$\hat{F}(n(c), c) \equiv \hat{F}(c) = 2\sqrt{\tilde{E}(c)\tilde{K}(c)} \tag{6}$$

The minimization of equation 6 with respect to c then gives :

$$\frac{d\tilde{E}(c)}{dc} \tilde{K}(c) + \tilde{E}(c) \frac{d\tilde{K}(c)}{dc} = 0 \tag{7}$$

Somewhat lengthy calculations show that, for $0 < c < 1$, equation 7 has a solution only for $1/2 < E^A_{Int}/E^Z_{Int} < 1$, in which case the unique solution is not a minimum. In fact, $\hat{F}(n, c, T = 0)$ is a surface with a downward facing concavity. Minimization of $\hat{F}(c)$ is then possible only for $c = 0$ (zigzag) and $c = 1$ (armchair). This corresponds to a phase separation between two different domains, separated by a line $E^Z_{Int} = 4E^A_{Int}/3$.

We now consider n and m as discrete quantities. As a result, two integers n_m and $n_m + 1$ can be defined as $n_m < \sqrt{\tilde{K}(c)/\tilde{E}(c)} < n_m + 1$ where $\sqrt{\tilde{K}(c)/\tilde{E}(c)}$ is the real minimum of

the continuous function $\hat{F}$. A two-phase coexistence is then observed when $\hat{F}(n_m, c, T = 0) = \hat{F}(n_m + 1, c, T = 0)$. For $c = 0$ and $c = 1$, this leads to vertical lines separated by $K/n(n+1)$ and horizontal lines separated by $K/3n(n+1)$, respectively, as presented in Figure 3-a of the main text.

(6,5) selectivity

Figure S1 displays the (n, m) dependence of the free energy, and the corresponding probability distribution, for interfacial energies stabilizing a $(6, 5)$ nanotube.

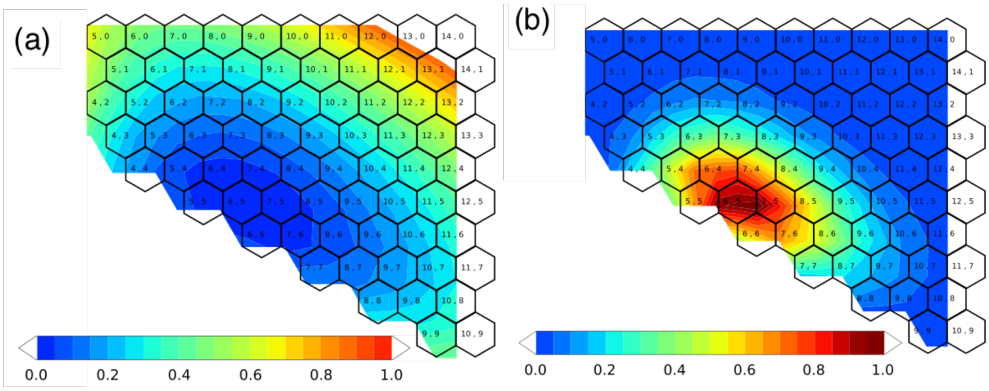

FIG. S1. (Color online) **a)** Example of (n, m) dependent contribution to the free energy $F(n, m) = E(n, m) - TS(n, m)$, calculated for $E^Z_{Int} = 250$ meV / bond and $E^A_{Int} = 150$ meV / bond and T = 973 K. **b)** Corresponding $P(n, m)$ probability distribution of chiralities. The minimum of $F(n, m)$ is set to zero, hence the maximum of $P(n, m)$ is equal to 1. In this example, the $(6, 5)$ chirality has the lowest $F(n, m)$, about 100 meV below $(7, 5)$.

Chirality Maps at different temperatures

Figure S2 shows the evolution of the chirality maps when increasing the temperature from 1000 to 1400 K.

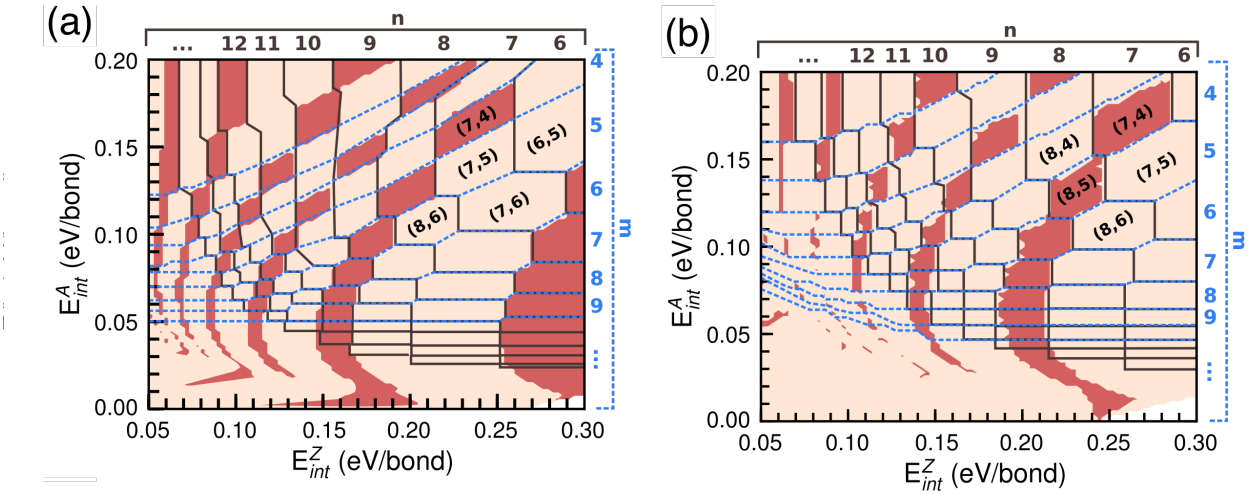

FIG. S2. (Color online) **a)** Chirality map at 1000 K. Iso-n (resp. iso-m) values are delimited by full black (resp. dashed blue) lines. Metallic tubes, for which $(n-m)$ is a multiple of 3, are shown in brick red, and semi-conducting ones are flesh-colored. The parameter space for armchair (metallic) and $(n, n-1)$ and $(n, n-2)$ (semi-conducting) tubes is larger than for other chiralities. **b)** Chirality map at 1400 K.

[1] P. Giannozzi, S. Baroni, N. Bonini, M. Calandra, R. Car, C. Cavazzoni, D. Ceresoli, G. L. Chiarotti, M. Cococcioni, I. Dabo, et al., Journal of Physics: Condensed Matter **21**, 395502 (2009).

[2] P. E. Blöchl, Phys. Rev. B **50**, 17953 (1994).

[3] J. P. Perdew, K. Burke, and M. Ernzerhof, Phys. Rev. Lett. **77**, 3865 (1996).